International Research Journal of Engineering and Technology (IRJET) e-ISSN: 2395-0056
Volume: 08 Issue: 01 | Jan 2021 www.irjet.net p-ISSN: 2395-0072

Comparative Study of EPLL and PL-EPLL Control Techniques for Grid-Connected SPV System

Kanchan Matiyali[1], S.K.Goel[2]

[1]Ph.D. Scholar, Dept. of Electrical Engineering, GBPUA&T, Pantnagar, Uttarakhand, India
[2]Professor, Dept. of Electrical Engineering, GBPUA&T, Pantnagar, Uttarakhand, India

---

Abstract - *This paper presents a comparative study of enhanced phase lock loop (EPLL) and pseudo linear EPLL (PL-EPLL) based control technique used for active power compensation of three-phase-grid-tied solar photovoltaic (SPV) system. Both EPLL and PL-EPLL are used for elimination of harmonics, balancing of load and control of dc link voltage at the point of common coupling (PCC). The performance of the whole system is tested under various conditions as load unbalancing, types of load, and varying irradiance SPV panel. A SPV system is connected to the three phase grid converting DC voltage into three phase AC by connecting a three phase two pulse voltage source converter (VSC). Under varying irradiance condition, to achieve maximum power from PV array, a Perturb and Observe (PnO) based maximum power point tracking (MPPT) algorithm is applied and gate pulse from the controller is given to the boost converter. Active power is controlled through the loss component of PV system and DC link voltage controller. The whole three-phase-grid-tied system is simulated in MATLAB/Simulink and the performance of the system is analyzed under various environmental and loading conditions. Results shows that dc link voltage is regulated with control of active power in the system and power quality of the system is maintained. A comparative analysis is also done based on THD in grid currents for both EPLL and PL-EPLL control techniques.*

Key Words: **Grid-tied system, PnO, active power compensation, EPLL, PL-EPLL**

1. INTRODUCTION

Due to limited availability and growing demand of electricity, conventional sources of energy such as, coal, hydro, petroleum, natural gas etc., there is urgent need to develop alternate sources such as renewable and sustainable sources of energy like solar, wind, bio-gas, and bio-mass. Hence applications of renewable energy sources are increasing tremendously. SPV system technology is famous out of all the other renewable energy technologies due to some advantages like this technology is pollution free, clean and green, requires less maintenance, freely available source and produces less emissions to our environment[1]. Therefore, the demand is increasing day by day for grid-tied and stand- alone PV systems.

SPV systems are interfaced with three phase grid through power electronics converters in the form of VSC; hence harmonics are injected in the system. These harmonics are caused by power electronic devices (IGBTs, diodes etc.), that generate poor power quality at point of common coupling (PCC). Power quality of the grid-connected system is governed by some power quality standards IEEE-519–1992, IEC-61000–3-2, 2000 [2], [3].

Under varying irradiance conditions, it is required to maximize the power of PV array. Various MPPT control techniques are used in the literature [4] so far like, Perturb and Observe (PnO), Incremental Conductance (InC), Hill Climbing, fractional open-circuit voltage, fractional short-circuit current, some intelligent control techniques like particle swan optimization (PSO), genetic algorithm (GA) and fuzzy logic (FL) based MPPT, and artificial neural network (ANN) based MPPT etc. Of all the MPPT techniques, PnO is the most widely used technique, simple in application, requires low calculations and low cost; however there are some drawbacks of PnO as it fails to track maximum power point (MPP) under sudden variation of environmental conditions and it cannot give results under partial shading conditions [5].

To compensate active power components in the grid-tied SPV system, fundamental current components are extracted from three phase load current. For this compensation various control techniques are published in literature like, Instantaneous reactive power (PQ) theory [6] synchronous reference frame (SRF) theory, power balance theory [7], SVPWM [8], SOGI techniques (Damped SOGI, SOGI-Q, SOGI-FLL), unity power factor (UPF) based [9], some adaptive techniques etc. [10]

In this paper EPLL and PL-EPLL techniques are used for the grid-tied SPV system. These control techniques are basically PLL techniques that are an advanced combination of phase detection, loop filter and voltage controlled oscillator. Constants in the internal loop of EPLL are decided from the literature [11].Output generated from solar PV array is provided to the boost converter though PnO MPP technique. This boost converter is further connected to three phase two pulse VSC which is basically a DC-AC voltage converter and then this VSC is connected to the three-phase-grid which feeds three-phase loads.

1.1 System description

Figure-1 shows a topology of two-stage three-phase-grid-tied PV system, which represents a solar PV array connected

to the DC-DC boost converter and a control pulse is provided to the converter from MPPT controller. A dc-link capacitor (C_{dc}) is connected with the solar PV array and the boost converter to stabilize the voltage generated from PV array. DC-DC boost converter is further connected to the three-phase two-pulse VSC having six IGBT switches (S_{a1}, S_{a2}, S_{b1}, S_{b2}, S_{c1}, and S_{c2}) which is further connected to three-phase-grid feeding three-phase loads.

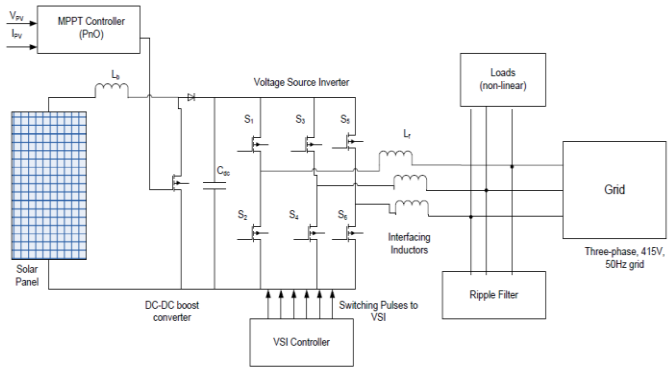

Figure-1: Schematic diagram of grid-connected SPV system

1.2 Selection of PV array

A 50kW SPV array is modelled in MATLAB/ Simulink by calculating number of series connected and parallel connected modules. We have selected a solar PV panel having open circuit voltage V_{oc} (32.9 V) and short circuit current I_{sc} (8.21A)

Maximum PV power is calculated as:

$$P_{mp} = (N_s * V_{mp})(N_p * I_{mp}) = 50kW$$

Where, N_p and N_s are parallel and series connected strings of selected PV module

$$P_{mp} = (N_s * 85\%\ of\ V_{oc})(N_p * 85\%\ of\ I_{sc})$$

From these equations, we can calculate number of series connected modules and parallel strings that are connected to form 50kW SPV array.

1.2.1 Selection of boost capacitor parameters

A DC-DC boost converter is connected with solar PV array with a dc link capacitor. The equivalent circuit of DC-DC boost converter is shown in figure. Value of boost inductor is calculated in normal temperature and irradiance conditions [12].

$$L_b = \frac{V_{mpp}\, d}{\Delta I\ f_{sw}} = 5mH$$

1.2.2 Voltage of DC bus and DC link capacitance:

DC-DC boost converter generates DC voltage which is further converted into three-phase AC to interface with grid. Hence value of DC link voltage is calculated as

$$V_{dc} = \frac{2\sqrt{2}V_{line-line}}{\sqrt{3}m} = 677.59\ V \approx 700V$$

Here, m is considered as 1. The equation of DC link voltage is expressed as

$$C_{dc} = \frac{(P_{dc}/V_{dc})}{2\omega V_{dcripple}} = 5416\ \mu F$$

1.2.3 Calculation of interfacing inductor of VSC

To eliminate high frequency components of currents in the VSC, interfacing inductors (L_f) are to be connected, the value of L_f is calculated using the expression,

$$L_f = \frac{\sqrt{3}m\ V_{dc}}{12\ h\ f_{sw}\Delta i} = 2.5mH$$

Where, h =1.2

2. Principle of control algorithm

The system consists of two controllers, one is PLL based control that is EPLL and PL- EPLL control, to provide pulses to three-phase VSC and another is MPPT control which provides gate pulse to the DC-DC boost converter.

2.1 MPPT Control

In this work a PnO based technique is used to extract maximum power from the solar PV array under varying environmental conditions. In this type of MPPT algorithm firstly, voltage and current sensed from the PV array and PV power is calculated, then a small change in the PV voltage or duty cycle of DC-DC boost converter is made and power is calculated. Both the powers are compared, if perturbation power is greater than the PV power, it is assumed that we are perturbing in the right direction and if it is lower, perturbation is done in reverse direction. Figure-2 shows the basic flowchart of the algorithm. This maximum voltage is further given to the pulse generator to generate pulse for the DC-DC boost controller [13].

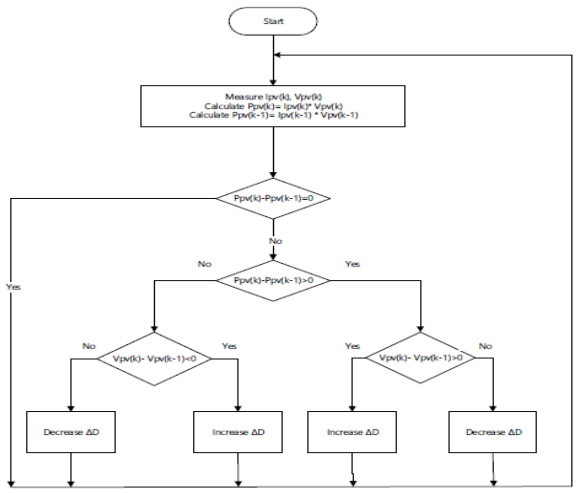

Figure-2: Flow chart of PnO based MPPT algorithm

2.2 EPLL control

EPLL is used to extract fundamental component of current from three-phase load current. Control of EPLL is presented in figure 3. This control is explained in the further sections:

2.2.1 Calculation of terminal voltage and unit templates

Voltage at PCC is measured and terminal voltage is calculated from the given expression [14]:

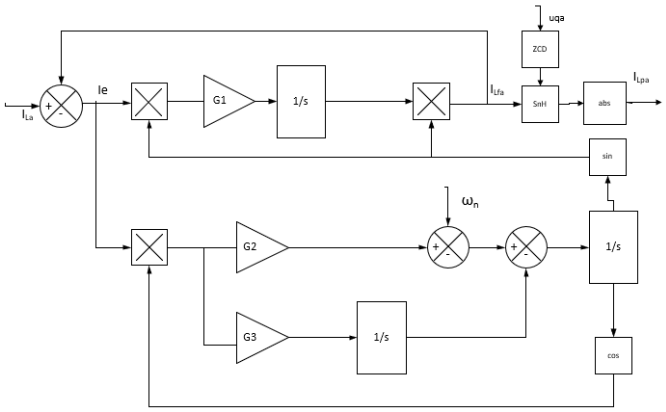

Figure-3: Schematic diagram of EPLL control technique

$$V_t = \sqrt{\frac{2}{3}\left(V_a{}^2 + V_b{}^2 + V_c{}^2\right)}$$

Where,

$$V_a = \frac{2V_{ab} + V_{bc}}{3}$$

$$V_b = \frac{-V_{ab} + V_{bc}}{3}$$

$$V_c = \frac{-V_{ab} - 2V_{bc}}{3}$$

Now, in-phase unit templates and quadrature unit templates can be calculated as:

$$u_{pa} = \frac{V_a}{V_t}$$

$$u_{pb} = \frac{V_b}{V_t}$$

$$u_{pc} = \frac{V_c}{V_t}$$

And,

$$u_{qa} = \frac{u_{pc} - u_{pb}}{\sqrt{3}}$$

$$u_{qb} = \frac{3u_{pa} + u_{pb} - u_{pc}}{2\sqrt{3}}$$

$$u_{qc} = \frac{-3u_{pa} + u_{pb} - u_{pc}}{2\sqrt{3}}$$

From figure-3, fundamental current component of three-phase load current (I_{Lfa}) is extracted for which we require I_{La}, in-phase unit templates u_{pa} and u_{qa} as input quantities, which are used to validate active power (I_{Lpa}). G_1, G_2 and G_3 are control gains which control the transients and steady state response in the system. With this technique, I_{Lfa} is extracted from I_{La}. A zero crossing detector (ZCD) is used to extract the amplitude of fundamental current component of three-phase load current and this ZCD also keeps I_{Lfa} in phase with V_a. Finally output to SCH is the amplitude of I_{Lfa} which is extracted from I_{La}.

2.2.2 Calculation of average active power component of load current

For load balancing, an average value of active power component is to be determined.

Table-1: Nomenclature of control parameters

P_{mp}= maximum power of SPV array	L_b= boost inductance
V_{mp}= voltage at maximum power	V_{dc}= DC link bus voltage
I_{mp}= current at maximum power	m= modulation index
V_{oc}= open circuit voltage	C_{dc}= DC link capacitance
I_{sc}= short circuit current	L_f= interfacing inductor
D= duty ratio of boost converter	H= overloading factor
ΔI= ripple current of boost	V_t= terminal voltage

converter	
F_{sw}= switching frequency of PWM	V_a, V_b, V_c= three phase instantaneous voltages at PCC
C_b= boost capacitance	V_{ab}, V_{bc}= line voltages
I_b= boost current	V_{dce}= error in DC link voltage
ΔV= peak ripple voltage	V_{dc_ref}= reference DC link voltage
I_{pvff}= PV feed forward term	I_{loss}= current loss component
I_p= average active component of load current	I_{pa}*, I_{pb}*, I_{pc}*= reference grid currents
U_{pa}, u_{pb},u_{pc}= in-phase unit templates	U_{qa}, u_{qb}, u_{qc}= quadrature phase unit templates

Hence, the average amplitude of active power component of load current is calculated as taking the average of amplitudes of fundamental load currents. This average current can be used in generation of three-phase reference currents which can further be used for generating switching pulses to the VSC. The average active power current component can be calculated as:

$$Ip = \frac{I_{pa} + I_{pb} + I_{pc}}{3}$$

2.2.3 Calculation of active power component of reference source current

To calculate amplitude of active power component of reference current, we use a PI controller. This PI controller is used to maintain dc link voltage. For controlling output voltage of VSC, dc link voltage should be greater than the peak of line voltage at point of common coupling (PCC). Input to this PI controller is an error signal which is difference between a reference dc link voltage (V_{dc_ref}) and dc link voltage tracked by MPPT controller.

$$V_{dce} = V_{dc\_ref} - V_{dc}$$

This error signal (V_{dce}) is passed through a PI controller which regulates the dc link voltage to its reference value which is fixed at 700V. Equation of PI controller is expressed as,

$$I_{loss}(k) = I_{loss}(k-1) + K_{pdc}[V_{dce}(k) - V_{dce}(k-1)] + K_{idc}V_{dce}(k)$$

Hence, net amplitude of active power component of reference current is expressed as:

$$I_p^* = I_p + I_{loss}$$

2.2.4 Calculation of reference grid currents

The reference grid currents are calculated from synchronization of unit templates and peak of measured reference grid currents, can be expressed as,

$$I_{pa}^* = I_p * u_{pa}, \quad I_{pb}^* = I_p * u_{pb}, \quad I_{pc}^* = I_p * u_{pc}$$

These reference grid currents are used to generate pulses to the three-phase-two-level VSC using hysteresis current controller. In this controller reference currents and current measured from the grid are compared and an error is generated. These error signals generate switching pulses to the VSC.

2.3 PL-EPLL control

This Control technique is also used to extract fundamental component of load current. The main advantage of using this control technique is that it doesn't need amplitude of load current [15] for extraction of fundamental component unlike in EPLL. Hence the controller becomes robust and efficient. The control technique is based on indirect control technique which directly uses reference grid currents to generate switching pulses to the VSC, and that doesn't change in frequent manner [16]. In this EPLL technique, fundamental load current I_{Lfa} is equal to the filtered value of I_{La}. The schematic diagram of PL-EPLL is shown in figure. Modified equations for PL-EPLL can be expressed as

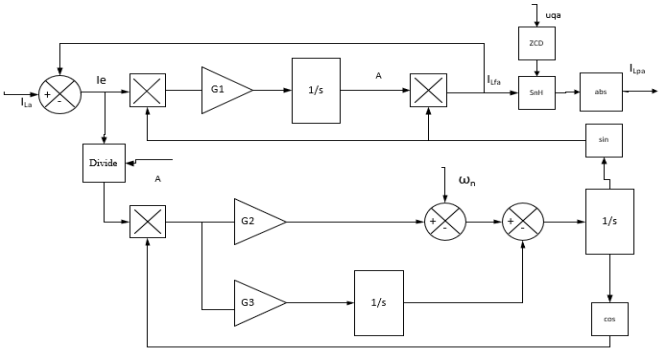

Figure-4: Schematic diagram of PL-EPLL control technique

$$\dot{A} = G_1 I_{ea} \sin \emptyset$$

$$\dot{\Delta\omega} = G_2 \frac{I_{ea}}{\dot{A}} \cos \emptyset$$

$$\emptyset = \omega_0 + \Delta\omega + G_3 \frac{I_{ea}}{A} \cos \emptyset$$

3. Simulation results

MATLAB/Simulink model for the 50kW grid connected SPV system is shown in figure-5. The system is tested under various environmental and loading conditions. Simulation parameters used for the whole grid connection system are given in table-2.

Three cases are considered for the simulation purpose.

a. Rapid change in irradiance of SPV array from 500W/m² to 700W/m² to 1000W/m²

b. Three phase linear load is made unbalanced at t= 0.6s and again balanced at t= 0.7s

c. Three phase non-linear load is made unbalanced at t= 0.6s and again balanced at t= 0.7s

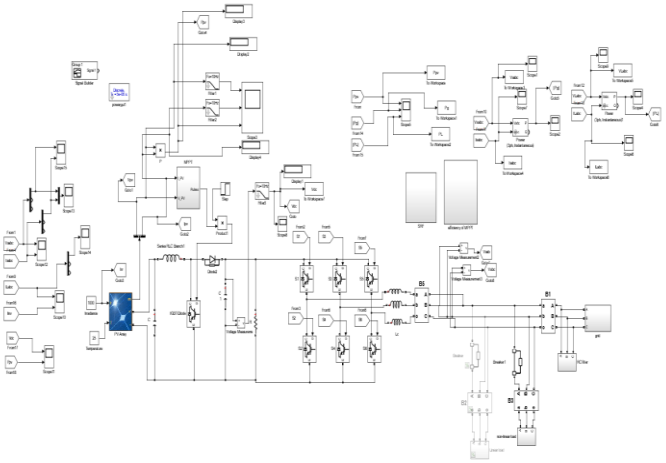

Figure-5: MATLAB/Simulink model of 50kW grid-connected system

Table-2: Simulation Parameters for grid-tied SPV system

Parameter	***Value***
Series connected modules (N_s)	22
Parallel connected modules (N_p)	11
Open circuit voltage (V_{oc})	32.9V
Short circuit current (I_{sc})	8.21A
Voltage at maximum power (V_{mp})	26.3V
Current at maximum power (I_{mp})	7.61A
Boost inductance (L_b)	5mH
DC link capacitance (C_{dc})	6000µF
Interfacing inductors (L_f)	2.5mH

For the first case, it can be observed from the simulation results for both EPLL and PL-EPLL control techniques that PV currents are increased as rapid change of irradiance and PV power is also increased according to the irradiance change. Grid voltages and grid currents are sinusoidal and grid currents change according to the change of irradiance. DC link voltage is controlled at fixed value of about 700V. Steady state oscillations are less in PL-EPLL as compared in EPLL.

For the second case, it can be seen from the results for both EPLL and PL-EPLL that grid voltages and grid currents are sinusoidal and grid current is in phase with the grid voltage. For the case of unbalanced linear load, only two phases are present and grid currents are increased to maintain total power. DC link bus voltage is controlled. Here PL-EPLL shows good dynamic response as compared to EPLL.

For the third case, under non-linear loading conditions, it can be seen that grid voltages and grid currents are again sinusoidal and grid current is in phase with the grid voltage. Load currents are non-sinusoidal due to the non-linear loading. For the unbalanced time period, grid currents are increased to maintain total power. DC link voltage is maintained at constant value of 700V. In this non-linear loading conditions dynamic response of PL-EPLL is excellent.

A comparison is done on the basis of THD in grid current, and THD in load current for the EPLL and PL-EPLL control techniques. The THD spectrum for EPLL and PL-EPLL under linear and non-linear loading conditions are shown in figure-12 and figure-13 respectively. The values for THDs are given in table-2.

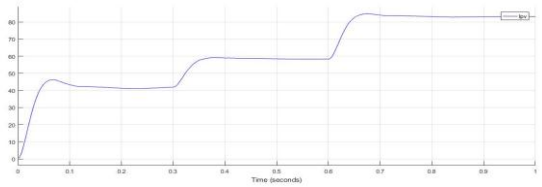

(a)

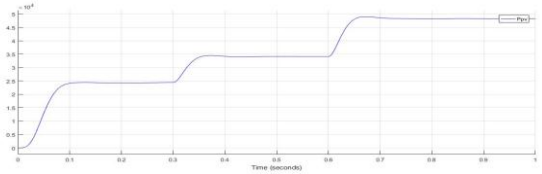

(b)

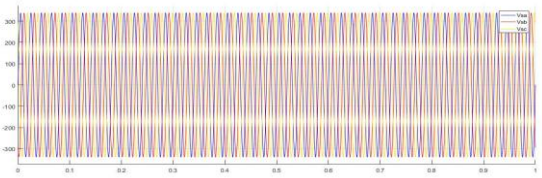

(c)

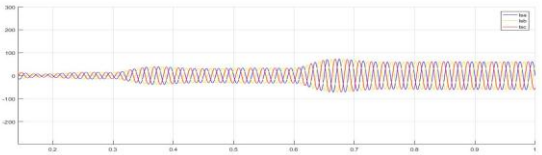

(d)

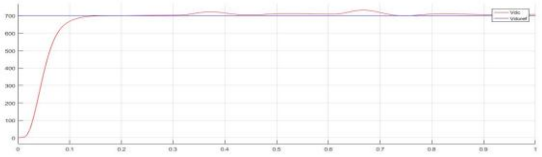

(e)

Figure-6: Simulation results for EPLL control under change in irradiance (a) PV current (b) PV power (c) three phase grid voltages (d) three phase grid currents (e) DC link bus voltage

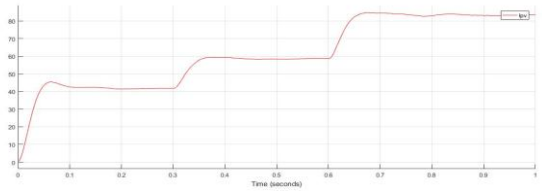

(a)

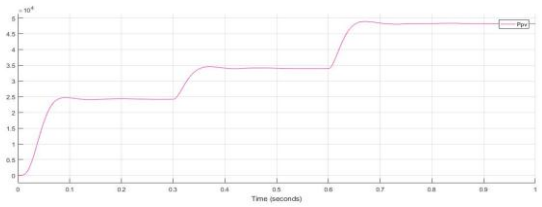

(b)

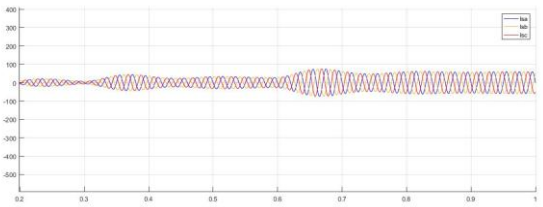

(c)

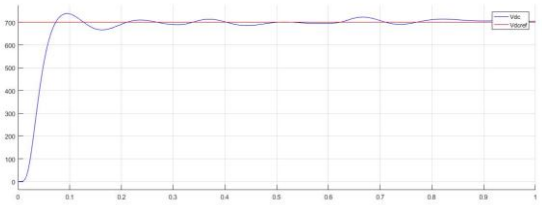

(d)

Figure-7: Simulation results for PL-EPLL control under change in irradiance (a) PV current (b) PV power (c) three phase grid currents (d) DC link bus voltage

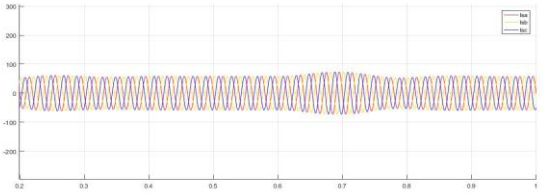

(a)

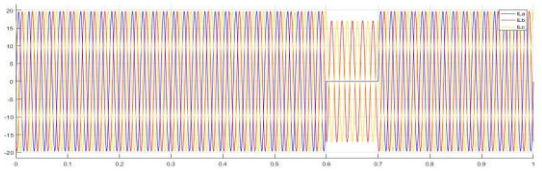

(b)

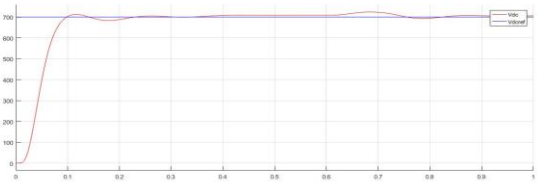

(c)

Figure-8: Simulation results for EPLL control under unbalanced linear load (a) grid currents (b) Load currents (c) DC link bus voltage

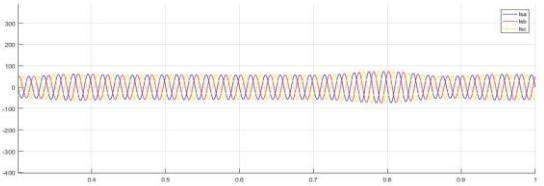

(a)

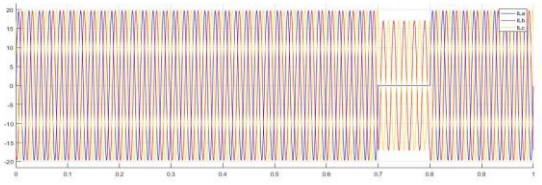

(b)

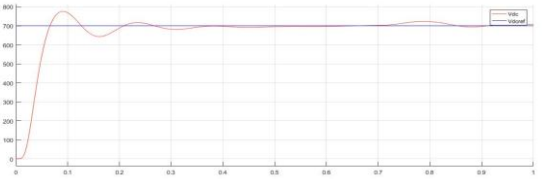

(c)

Figure-9: Simulation results for PL-EPLL control under unbalanced linear load (a) grid currents (b) Load currents (c) DC link bus voltage

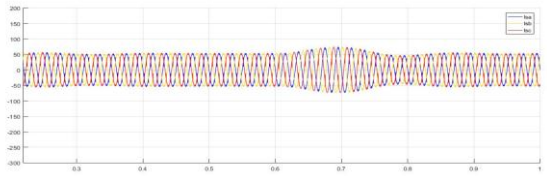

(a)

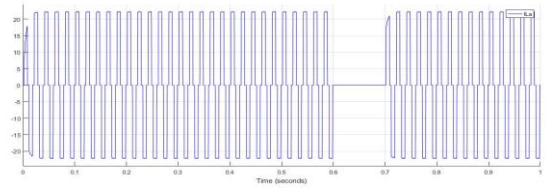

(b)

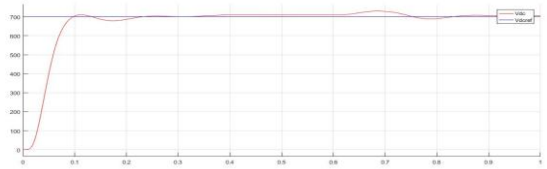

(c)

Figure-10: Simulation results for EPLL control under unbalanced non- linear load (a) grid currents (b) Load current of phase 'a' (c) DC link bus voltage

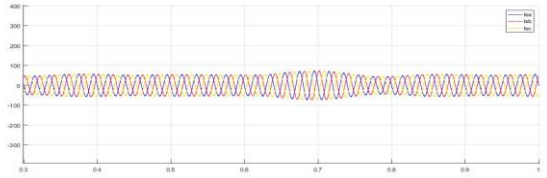

(a)

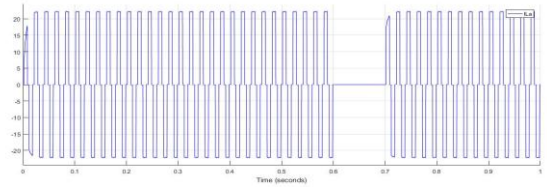

(b)

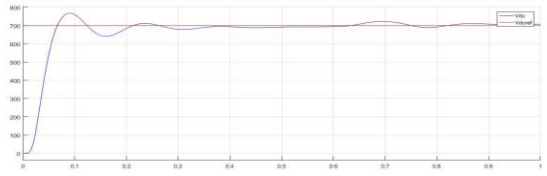

(c)

Figure-11: Simulation results for PL-EPLL control under unbalanced non- linear load (a) grid currents (b) Load current of phase 'a' (c) DC link bus voltage

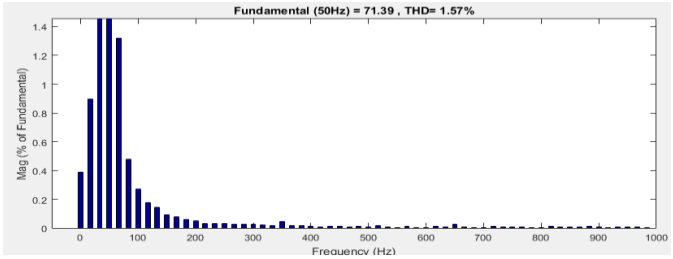

(a)

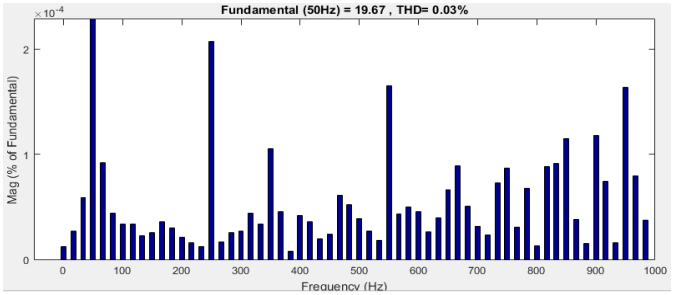

(b)

Figure-12: THD in (a) grid current (b) load current for EPLL technique under linear loading

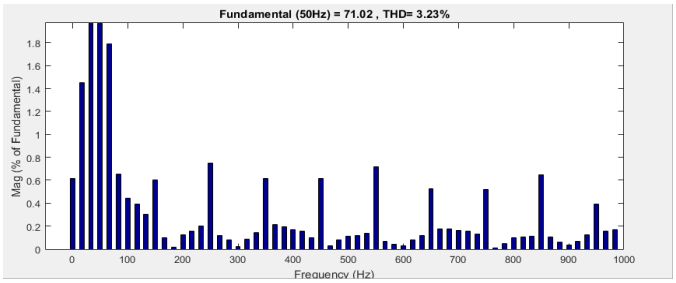

(a)

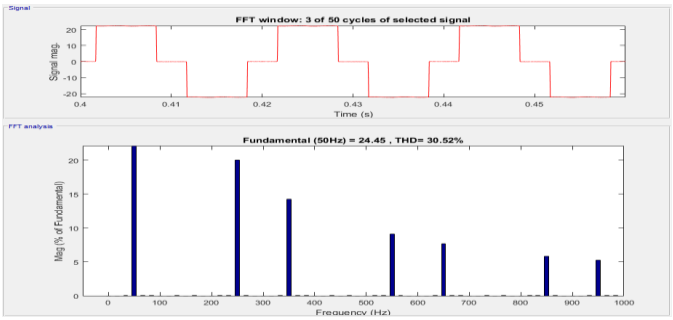

(b)

Figure-13: THD in (a) grid current (b) load current for EPLL technique under non-linear loading

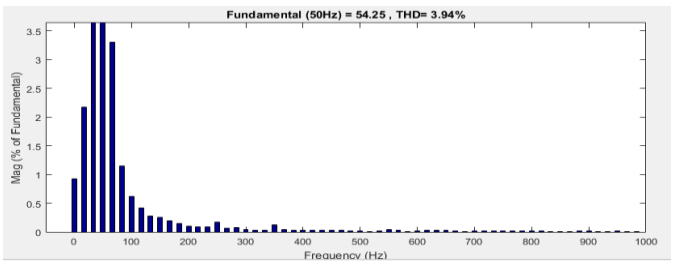

(a)

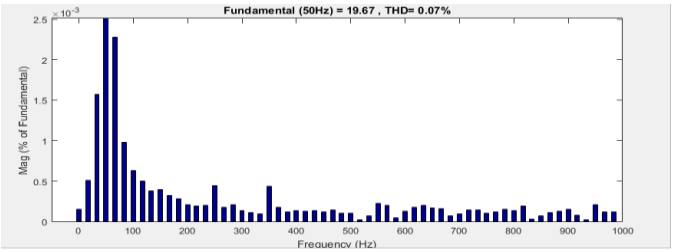

(b)

Figure-14: THD in (a) grid current (b) load current for PL-EPLL technique under linear loading

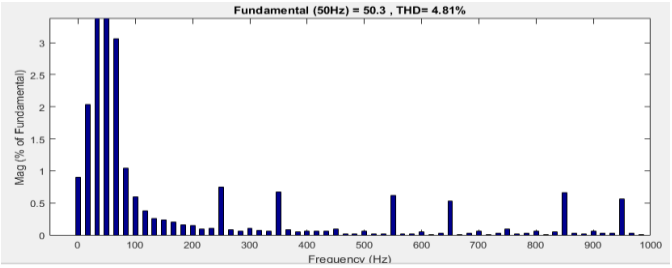

(a)

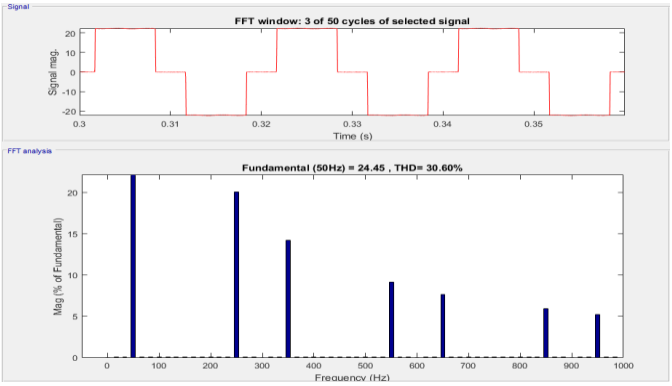

(b)

Figure-15: THD in (a) grid current (b) load current for PL-EPLL technique under non- linear loading

Table-3: Summary of results under various conditions

Test cases under consideration	*THD of I_{sa} (in %)*		*THD of I_{La} (in %)*	
	EPLL	*PL-EPLL*	*EPLL*	*PL-EPLL*
Unbalanced linear load	1.57	3.94	0.03	0.07
Unbalanced non-linear load	3.23	4.81	30.52	30.62

4. CONCLUSIONS

Control technique based analysis has been done on the three phase grid connected solar PV system and performance of the whole system has been analyzed for elimination of harmonics, load balancing and correction of power factor. The control techniques which have analyzed for the comparison purpose are EPLL and improved EPLL techniques. Both techniques are used for extraction of fundamental component of three phase load currents. DC component error has been eliminated in improved EPLL technique. Also this improved EPLL control technique has been used to reduce load unbalancing. The summary of results for the grid-connected solar PV system under various parameters is shown in table-3 on the basis of total harmonic distortion (THD). It can be found that THD in grid currents are according to IEEE-519 standards (under 5%) even under non-linear loading conditions.

REFERENCES

1. M. Ameli, S. Moslehpour, and M. Shamlo, 2008. “Economical load distribution in power networks that include hybrid solar power plants,” Elect. Power Syst. Res., vol. 78, no. 7, pp. 1147–1152.
2. IEEE Recommended Practices and requirement for Harmonic Control on electric power System, 1992. IEEE Standard 519.
3. Limits for Harmonic Current Emissions, 2000 IEC-61000–3-2, Int. Electrotech. Comm.
4. Mohan, N., Undeland, T. M., & Robbins, W. P. 2003. Power electronics: converters, applications, and design. John wiley & sons.
5. M. Killi, and S. Samanta, 2015. “Modified Perturb and Observe Algorithm for Drift Avoidance in Photovoltaic Systems,” vol. 0046, no. c, pp. 1-10.
6. Akagi H, Watanabe EH. M Aredes. 2007. Instantaneous power theory and applications to power conditioning. New Jersey, USA: John Wiley & Sons.
7. Singh Bhim, Chandra Ambrish, Al-Haddad Kamal, Anuradha, Kothari DP., 1998. Reactive power compensation and load balancing in electric power distribution systems. Int J Electr Power Energy Syst; 20(6):375–81.
8. Zhou Juan, Wu Xiao-jie, Geng Yi-wen, Dai Peng., 2007. Simulation research on a SVPWM control algorithm for a four-leg active power filter. J China Univ Mining Technol 17(4):590–4.
9. M. Kumar, N. Gupta and R. Garg, 2016. "Unity power factor control of grid connected SPV system using instantaneous symmetrical component theory," IEEE 1st International Conference on Power Electronics, Intelligent Control and Energy Systems (ICPEICES), Delhi, 2016, pp. 1-6.
10. M. I. Milan´es, E. R. Cadaval, and F. B. Gonz´alez, 2007. “Comparison of control strategies for shunt active power filters in three-phase four-wire systems,” IEEE Trans. Power Electron., vol. 22, no. 1, pp. 229–236.
11. M. K. Ghartemani, H. Mokhtari, M. R. Iravani, and M. Sedighy, 2004. “A signal processing system for extraction of harmonics and reactive current of single-phase systems,” IEEE Trans. Power Del., vol. 19, no. 3, pp. 979–986.

12. Verma, A. K., Singh, B., and Shahani, D. T., 2012. "Grid interfaced solar photovoltaic power generating system with power quality improvement at AC mains," Proceedings of the IEEE International Conference on Sustainable Energy Technologies, Nepal, 24–27 ,pp. 177–182.
13. Atallah, A. M., Abdelaziz, A. Y., & Jumaah, R. S. 2014. Implementation of perturb and observe MPPT of PV system with direct control method using buck and buck-boost converters. Emerging Trends in Electrical, Electronics & Instrumentation Engineering: An international Journal (EEIEJ), 1(1), 31-44.
14. Sharma, S., & Singh, B. 2011. An enhanced phase locked loop technique for voltage and frequency control of stand-alone wind energy conversion system. In India International Conference on Power Electronics 2010 (IICPE2010) (pp. 1-6). IEEE.
15. Karimi-Ghartemani, M. 2013. Linear and pseudolinear enhanced phased-locked loop (EPLL) structures. IEEE transactions on industrial electronics, 61(3), 1464-1474.
16. Singh, B. 2018. Grid synchronization control for an autonomous PV-wind-battery based microgrid. In 2018 IEEMA Engineer Infinite Conference (eTechNxT) (pp. 1-6). IEEE.